Size Dependence of the Multiple Exciton Generation Rate in CdSe Quantum Dots

Zhibin Lin,[†,‡,*] Alberto Franceschetti,[‡,*] and Mark T. Lusk[†,*]

[†]Department of Physics, Colorado School of Mines, Golden, Colorado 80401, United States and [‡]National Renewable Energy Laboratory, Golden, Colorado 80401, United States

ABSTRACT The multiplication rates of hot carriers in CdSe quantum dots are quantified using an atomistic pseudopotential approach and first-order perturbation theory. We consider both the case of an individual carrier (electron or hole) decaying into a trion and the case of an electron–hole pair decaying into a biexciton. The dependence on quantum dot volume of multiplication rate, density of final states, and effective Coulomb interaction are determined. We show that the multiplication rate of a photogenerated electron–hole pair decreases with dot size for a given absolute photon energy. However, if the photon energy is rescaled by the volume-dependent optical gap, then smaller dots exhibit an enhancement in carrier multiplication rate for a given relative photon energy. We find that holes have much higher multiplication rates than electrons of the same excess energy due to the larger density of final states (positive trions). When electron–hole pairs are generated by photon absorption, however, the net carrier multiplication rate is dominated by electrons because they have much higher excess energy on average. We also find, contrary to earlier studies, that the effective Coulomb coupling governing carrier multiplication is energy-dependent.

KEYWORDS: multiple exciton generation · carrier multiplication · CdSe nanocrystal quantum dots · photovoltaic · pseudopotential method · Fermi's golden rule

Semiconductors typically produce a single electron–hole pair per photon absorbed. The excess photon energy $\hbar\omega - E_{gap}$ (where ω is the photon frequency and E_{gap} is the semiconductor band gap) is converted to heat and represents a net loss for the photoconversion efficiency. It is theoretically possible, however, for a photon of sufficiently high energy to generate two or more lower energy electron–hole pairs in a process known as multiple exciton generation (MEG). This process is illustrated in Figure 1. Provided that MEG occurs faster than competing carrier relaxation processes, more than one pair of charge carriers can be collected per photon absorbed. Thus, in addition to its fundamental physics interest, MEG raises the prospect of designing solar cell devices that utilize high energy photons with greater efficiency than is currently possible.

Early work in this area[1,2] suggested that the MEG process is enhanced by quantum confinement of carriers, motivating experimental investigations of MEG in a variety of nanostructured materials.[3−23] Initial reports of very high MEG yields in PbSe, PbS, and CdSe nanocrystal quantum dots (QDs)[3−5,23] were followed by a critical analysis of the assumptions used to extract the MEG yield from optical spectroscopy measurements.[15,16,21,24] The consequences of the energy dependence of the absorption cross section,[15] the nonlinear dependence of the bleaching ratio on the number of excitons,[24] and the nonradiative recombination of charged excitons[16] on the accuracy of MEG measurements have all been discussed in the literature. This has led to a reassessment of earlier experimental results.

A controversy has recently emerged, though, as to how much, if at all, quantum confinement really enhances the MEG process. Most experimental investigations of MEG in nanostructures have focused on the *quantum yield* (QY), defined as the average number of excitons produced per absorbed photon. MEG manifests itself by generating more than one exciton per photon (QY > 1) when the photon energy exceeds a certain threshold, $\hbar\omega_{th}$. Experiments for PbSe[3] and Si[10] nanocrystals suggested that the QY measured at a given *absolute* photon energy decreases when the nanocrystal size decreases, while other experiments have reported a weak and/or nonmonotonic dependence of the QY on size.[14] When measured at a given *relative* photon energy, $\hbar\omega/E_{gap}$, the QY was shown to increase as the nanocrystal volume decreases.[3,4,10,11] Rabani *et al.*[25,26] calculated the QY of a set of small CdSe, InAs, and Si nanocrystals and found an increase as the size decreases. First-principle quantum chemistry calculations have been utilized to confirm the ultrafast generation of multiexcitons in small PbSe, CdSe, and Si clusters.[27−29,31] A few experimental[10,14,16,19] and theoretical[19,32]

* Address correspondence to zlin@mines.edu, alberto.franceschetti@nrel.gov, mlusk@mines.edu.

Received for review August 17, 2010 and accepted February 28, 2011.

Published online February 28, 2011
10.1021/nn200141f

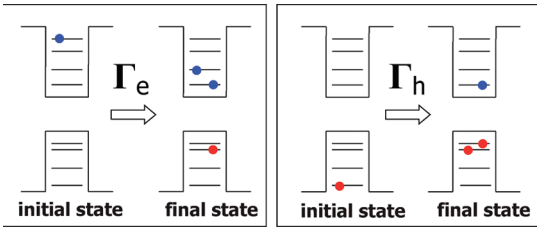

Figure 1. Schematic diagram of MEG decay paths for an excited electron (left) and an excited hole (right). Several degenerate final state configurations may exist and may contribute to the MEG decay rate.

investigations have also attempted a comparison of the QY of QDs *versus* bulk semiconductors. Beard *et al.*[10] reported a significantly higher QY in Si nanocrystals than in bulk Si at the same relative photon energy. However, Nair *et al.*[14] found that the QY of PbS nanocrystals is lower than that of PbS cystalline films[33] when measured at fixed absolute photon energy. Similar results were reported[19,21,32] for PbSe nanocrystals.

The implications of these results for the photoconversion efficiency of solar cells utilizing the MEG effect have been recently debated. McGuire *et al.*[21] defined the MEG *efficiency* as the product of the QY times the band gap ("energetic" figure of merit) and argued that the MEG efficiency is more relevant to the photoconversion process than the MEG QY. Delerue *et al.*[32] defined the MEG *energy efficiency* as the ratio between the total excitonic energy (the average number of generated excitons times the energy gap) and the photon energy. They showed that the MEG energy efficiency increases as the nanocrystal volume decreases,[21,32] even when measured at fixed absolute photon energy. Beard *et al.*[47] submitted that the MEG efficiency is proportional to the slope of the QY *versus* the relative photon energy $\hbar\omega/E_{gap}$ (above the MEG threshold $\hbar\omega_{th}$). The dependence of the QY on QD volume calculated at fixed relative photon energy is therefore more appropriate to describe the trend of the MEG efficiency with quantum dot size.

Unfortunately, it is difficult to extract information on the relevance of quantum confinement to the MEG process from experimental measurements of the QY. The reason is that the QY depends on the ratio of the MEG rate, Γ_{MEG}, and the total exciton decay rate, Γ_{tot}. The latter includes contributions from competing decay processes, such as phonon-assisted carrier cooling. Since both Γ_{MEG} and Γ_{tot} depend on the nanostructure size (as well as the photon energy), the observation of a certain dependence of the QY on size does not necessarily imply that the same trend exists for Γ_{MEG}. Thus, it would be very useful to quantify the size dependence of the MEG *rate* itself. This quantity is difficult to measure experimentally, but accurate calculations of Γ_{MEG} as a function of size have recently become available[25,26,42] and can provide information on multiexciton dynamics and clarify the role of quantum confinement in the MEG process.

Nair *et al.*[14] argued that this quantity should not exhibit any volume dependence because of the offsetting volume dependencies of single exciton and biexciton Coulomb coupling (V^{-4}) and the biexciton density of states (V^4). Their reasoning was based on a simple phenomenological model, and it would be particularly useful to provide a more quantitative analysis for a system for which a realistic electronic structure can be calculated. Kane[41] has studied the impact ionization rate in bulk Si by first-order time-dependent perturbation theory, and Allan *et al.*[42] have recently compared the MEG rates of bulk PbSe and PbSe QDs using tight-binding calculations. Rabani *et al.*[25,26] applied the pseudopotential approach for CdSe, InAs, and Si nanocrystals and decomposed the MEG rate into the trion density of states and average Coulomb coupling. While the size dependence of the Coulomb coupling was considered in refs 25 and 26, no quantitative comparison of volume scaling for the MEG rate, trion density of states, and effective Coulomb coupling has ever been carried out.

Here we use atomistic pseudopotential calculations and first-order perturbation theory to quantify the dependence of the MEG rate on photon energy and nanoparticle volume for zinc blende CdSe nanocrystalline QDs. The perturbative approach assumes that the relaxations can be viewed as incoherent, and this is reviewed elsewhere.[26] In this study, the volume dependence of the MEG rate is decomposed to show the relative contributions of Coulomb matrix elements and density of final states. We find that (i) the MEG rate increases rapidly with the excess energy of the carriers; (ii) at fixed *absolute* photon energy, the MEG rate of a photogenerated electron−hole pair decreases as the volume of the QD decreases; and (iii) at fixed *relative* photon energy, the MEG rate increases as the volume decreases.

RESULTS

MEG Rate of Individual Charge Carriers. We consider here four nearly spherical CdSe QDs: $Cd_{216}Se_{213}$ (D = 2.9 nm), $Cd_{312}Se_{321}$ (D = 3.2 nm), $Cd_{484}Se_{495}$ (D = 3.7 nm), and $Cd_{784}Se_{739}$ (D = 4.3 nm), where D is the QD diameter. The MEG rate is calculated using Fermi's golden rule (see Methods section). Figure 2 shows the calculated MEG rates of electrons and holes for 2.9 and 3.7 nm QDs. The transition rates of individual electron or hole initial states to final trion states are plotted in this figure as a function of the absolute electron/hole energy measured with respect to the vacuum level (Figure 2a,b), as well as the relative electron/hole excess energy $|E-E_0|/E_{gap}$ (Figure 2c,d). Here E_0 is the conduction band minimum (CBM) in the case of electrons and the valence band maximum (VBM) in the case of holes, and the optical gap E_{gap} is calculated as $E_{gap} = \varepsilon_{CBM} - \varepsilon_{VBM} - J_{VBM,CBM}$, where ε_{CBM} and ε_{VBM} are the single-particle energies of the CBM

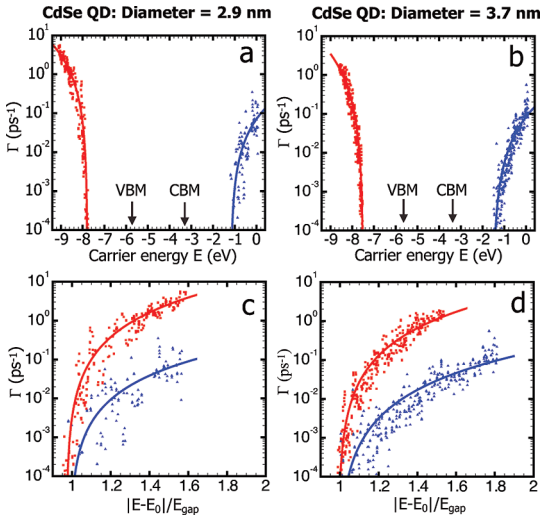

Figure 2. Calculated MEG rate as a function of the electron and hole energy for CdSe QDs with diameters of 2.9 nm (left) and 3.7 nm (right). Energies are shown in two ways: (a,b) with respect to the vacuum level; (c,d) with respect to the band edge energy E_0 (CBM for electrons and VBM for holes) and rescaled by the optical band gap E_{gap}. Each symbol corresponds to the transition rate of individual electron (blue) or hole (red) initial states to final trion states. The solid lines represent a fit of the energy dependence $\Gamma(E)$ of the MEG rate, as discussed in the text. Arrows indicate the positions of the CBM and VBM.

TABLE 1. Fitted Parameters for the Energy Dependence of Electron and Hole MEG rates of Equation 1[a]

diameter (nm)	α_h	α_e
2.9	2.3	2.1
3.2	2.4	2.3
3.7	2.7	2.5
4.3		2.6

[a] For the largest QD (4.3 nm), we show only α_e due to the significant computational cost required to calculate the hole MEG rate.

and VBM, respectively, and $J_{VBM,CBM}$ is the screened Coulomb energy between VBM and CBM (see Methods section). The MEG rates of electron and holes are seen to increase rapidly with excess energy. For the same relative excess energy, excited holes have transition rates more than an order of magnitude greater than excited electrons.

Data such as that shown in Figure 2 were generated for all four QDs. The transition rates of individual electron and hole initial states to final trion states were subjected to an arithmetic average of initial states within a 100 meV energy window. The resulting averaged transition rates were then used for the fitting of the energy dependence of the electron and hole MEG rates to a power law:

$$\Gamma_{h,e}(E) = A_{h,e}(E - E_{th})^{\alpha_{h,e}} \quad (1)$$

where the threshold energy E_{th} is the ground-state energy of a negative trion (for electrons) or a positive

TABLE 2. Fitted parameters for the Volume Dependence of Electron and Hole MEG Rates of Equation 2

E (eV)	β_h	B_h	E (eV)	β_e	B_e
−7.8	−2.0	−11.2	−0.6	−1.8	−0.93
−8.0	−2.4	−66.8	−0.7	−1.7	−0.78
−8.2	−2.2	−69.7	−0.8	−1.6	−0.60
−8.4	−2.3	−128.0	−0.9	−1.2	−0.18

trion (for holes). As shown in eq 11 and eq 12 in the Methods section, the threshold energy can be computed from the energies of the constituent electrons and holes in the ground-state trions together with the corresponding screened Coulomb energies. Table 1 summarizes the values of α_h and α_e extracted from the fit. We find that α varies between 2.1 and 2.7, depending on the QD size, and is slightly larger for holes than for electrons.

The volume dependence of the MEG rates was calculated for a set of given electron and hole energies and fitted to the function

$$\Gamma_{h,e}(V) = \Gamma^0_{h,e} + B_{h,e}V^{\beta_{h,e}} \quad (2)$$

where $B_{h,e}$ and $\beta_{h,e}$ are listed in Table 2. In particular, $\beta_{h,e}$ ranges between −2.0 and −2.4 for holes (depending on their energy) and between −1.2 and −1.8 for electrons. The negative sign of the parameters $B_{h,e}$ and $\beta_{h,e}$ (both for electrons and for holes) indicates that for a given carrier energy, E, the MEG rate decreases as the QD volume decreases.

The calculated MEG rates $\Gamma(E)$ of the four QDs considered here are shown in Figure 3a. In order to explain the trends with energy and volume, the MEG rate was decomposed (following refs 25, 26, 45, and 46) into the trion density of states (DOS) contribution, $\rho(E) = \sum_f \delta(E - E_f)$, and the effective Coulomb coupling contribution, $|\bar{W}|^2 = \hbar\Gamma(E)/2\pi\rho(E)$. These two components are shown in Figure 3b,c, respectively. The trion DOS (Figure 3b) shows an energy dependence very similar to the overall MEG rate (Figure 3a); that is, the number of final trion states increases rapidly as the excess energy increases. While this trend holds for trions deriving from both holes and electrons, for a given excess energy, the positive trion DOS is significantly larger than the negative trion DOS, as shown in the inset plot of Figure 3b for a 3.7 nm dot. This is because the manifold of hole states is much denser than its electron counterpart. As a result, the number of available trion states, for a given excess energy, is much higher for holes than electrons, and this dominates the overall MEG rates. Previous calculations using an atomistc pseudopotential approach for PbSe QDs have revealed a dense feature of valence states.[45] In the case of CdSe QD, the asymmetry in the density of states between the conduction and valence states is even more pronounced.

The effective Coulomb coupling, $|\bar{W}|^2$ (Figure 3c), peaks just above the threshold energy and then exhibits a

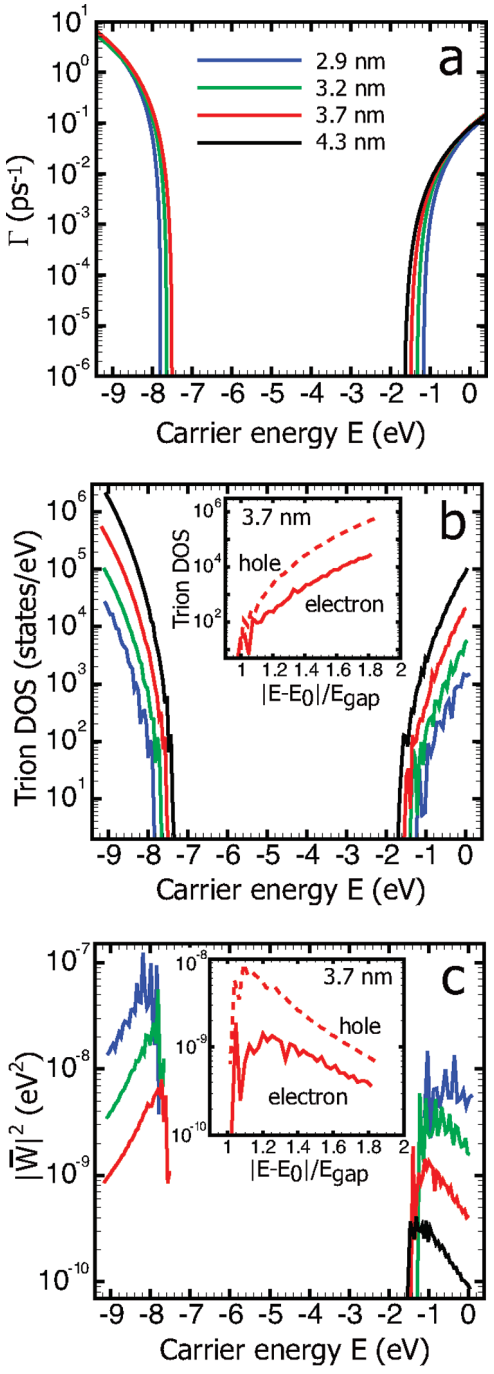

Figure 3. (a) MEG rate $\Gamma(E)$, (b) trion DOS $\rho_{trion}(E)$, and (c) effective Coulomb coupling, $|\bar{W}|^2(E)$, as functions of the electron and hole energy for four CdSe QDs. Insets in (b) and (c) show the trion DOS and the effective Coulomb coupling for a 3.7 nm QD as a function of the relative energy rescaled by the optical band gap. The MEG rates are fitted as described in the text using eq 1. The trion DOS is obtained using a Gaussian broadening of 10 meV. For the largest dot (4.3 nm), the MEG rate and effective Coulomb coupling are only shown for electrons due to the significant computational cost required to calculate MEG rates from the large set of possible positive trion configurations.

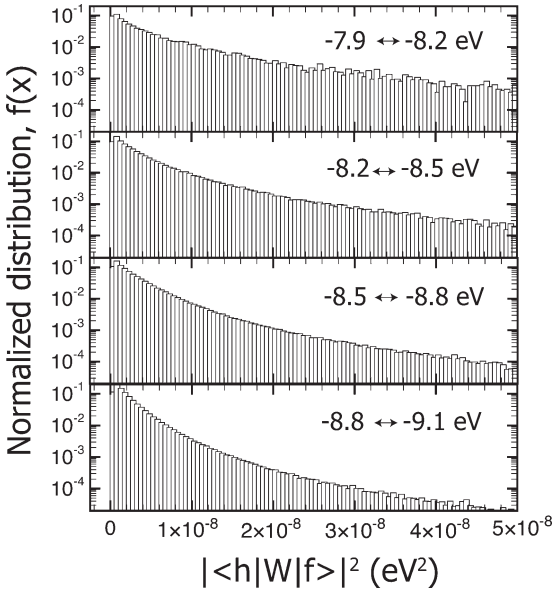

Figure 4. Normalized distribution of Coulomb matrix elements $|\langle h|W|f\rangle|^2$ of the holes states in a 3.2 nm CdSe dot within four energy windows (top to bottom).

decay as the excess energy increases. The decay becomes faster as the size of the QD increases and is more pronounced for holes than for electrons. This trend holds for all four QDs and is in contrast to the assumptions and conclusions of earlier studies. Specifically, a constant Coulomb coupling was assumed for an examination of impact ionization in bulk Si,[41] and a recent tight-binding study concluded that there is only a weak energy dependence in the Coulomb coupling for PbSe QDs.[46] Recent pseudopotential calculations for CdSe QDs[25,26] found that the Coulomb coupling has no energy dependence for dots up to 3.0 nm. Our calculations suggest that this is not the case for larger QDs. In any case, the downward trend in the energy dependence of the Coulomb coupling is overshadowed by the opposing trend in the trion DOS. The size dependence of the effective Coulomb coupling was obtained by fitting the data for all four CdSe QDs to a power law: $|\bar{W}|^2 \propto V^{\gamma}$, with γ ranging from -2.6 to -3.2 for electrons and -3.6 to -4.0 for holes.

The energy distribution of the Coulomb matrix elements sheds light on the reason why the effective Coulomb coupling decreases with increasing excess energy. The absolute number of Coulomb matrix elements with a relatively large amplitude increases slightly with excess energy, but the fraction of such states significantly decreases with excess energy. This is shown in Figure 4 for a 3.2 nm CdSe QD. The distributions have been fitted to an exponential decay function, $f(x) \propto \exp(-x/\lambda)$, with the parameter λ showing the similar decreasing trend as in $|\bar{W}|^2$. While the denser trion manifold at higher excess energy (Figure 2b) points to an increasing number of possible channels for the MEG decay, most of these transitions exhibit a weak Coulomb coupling; that is, they have small Coulomb matrix elements. Thus, the fraction of small Coulomb matrix elements on average increases with

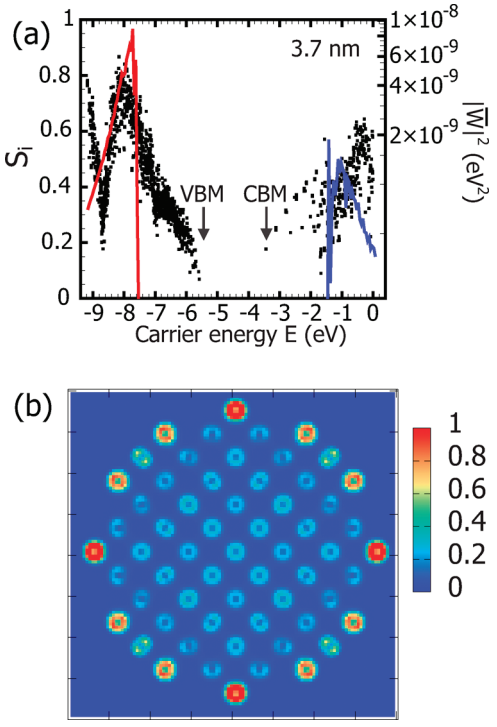

Figure 5. (a) Surface projection fraction, S_i, of the single-particle wave function norm plotted as a function of the electron and hole energy. Each point corresponds to a single-particle eigenstate. The surface region is defined as the set of points closer than R_{WS} (the Wigner−Seitz radius of bulk CdSe) from at least one surface Cd/Se atoms. The effective Coulomb coupling, $|\bar{W}|^2$, is shown (solid line) for the region where MEG occurs. (b) Charge density distribution (arbitrary units) of hole states between −8.0 and −7.5 eV of a 3.7 nm CdSe QD, plotted on a (001) plane.

increasing excess energy (Figure 4), leading to a weaker average Coulomb coupling (Figure 2c). For small QDs, this dependence is less evident due to a smaller number of trion states involved in MEG processes. This is clear, for instance, in our results for electrons in a 2.9 nm CdSe QD (Figure 2) and in earlier studies which found no energy dependence in CdSe of similar small sizes.[25,26]

In order to investigate the effect of surface localization on the MEG rate, we have computed the spatial distribution of the initial-state electron and hole wave functions. For each single-particle state i of a given QD, we calculated the fraction of the wave function norm that resides in the surface region of the QD, $S_i = \int_{\mathbf{r}\in S}|\psi_i(\mathbf{r})|^2 d\mathbf{r}$, where S is a thin shell around the surface of the QD. Figure 5 shows S_i (Figure 5a) and the charge density distribution of hole states located between −8.0 and −7.5 eV (Figure 5b) for the 3.7 nm CdSe QD. The plot of S_i (Figure 5a) indicates that states near the band edges are localized in the core of the QD. As the energy level moves away from the band edges, though, the wave functions spread to occupy a larger portion of the surface shell. The broad peak located 3 eV below the VBM originates from surface states associated with the ligands used to passivate the QD surface (see Figure 5b). These results are consistent with recent first-principles calculations for $Cd_{33}Se_{33}$ clusters passivated by amines and phosphine oxide ligands.[30] Also shown in Figure 5a is the Coulomb coupling $|\bar{W}|^2$ of the 3.7 nm QD. In the case of electrons, $|\bar{W}|^2$ decreases as the surface projection, S_i, increases. However, this is not the case for holes. They exhibit large values of $|\bar{W}|^2$ even when their wave functions are largely localized near the surface of the QD (Figure 5b). The results of Figure 5 suggest that there is no obvious correlation between $|\bar{W}|^2$ and the core/surface projection of the wave functions; surface localization of the wave functions does not appear to have a significant effect on the MEG rate. The dependence of the MEG *quantum yield* on the type of surface passivation, reported, for example, by Beard *et al.*,[18] appears to be related to the effects of passivation on competing decay channels for the photoexcited electron−hole pair.

MEG Rate of an Electron−Hole Pair. Having discussed the MEG rates of individual electrons and holes, we now consider the rate at which an electron−hole pair decays into a biexciton. Because many-body selection rules forbid the simultaneous transition of the electron and the hole (within first-order perturbation theory), the MEG rate of an electron−hole pair (e,h) is simply the sum of the MEG rates of the electron and the hole: $\Gamma(e,h) = \Gamma_e + \Gamma_h$. When a QD is excited by a laser pulse, different transitions that are nearly degenerate in energy can be excited. Thus, we calculate the MEG rate for a photon of energy $\hbar\omega$, as

$$\Gamma(\hbar\omega) = \sum_e p_e(\hbar\omega)\Gamma_e + \sum_h p_h(\hbar\omega)\Gamma_h \qquad (3)$$

where

$$p_h(\hbar\omega) = \frac{\sum_c |M_{h,c}|^2 \delta(E_{h,c} - \hbar\omega)}{\sum_{v,c} |M_{v,c}|^2 \delta(E_{v,c} - \hbar\omega)} \qquad (4)$$

$$p_e(\hbar\omega) = \frac{\sum_v |M_{v,e}|^2 \delta(E_{v,e} - \hbar\omega)}{\sum_{v,c} |M_{v,c}|^2 \delta(E_{v,c} - \hbar\omega)} \qquad (5)$$

The quantity p_h (p_e) is the probability of creating a hole in the valence state v (an electron in the conduction state c) as a result of the absorption of a photon of energy, $\hbar\omega$. The integral $M_{v,c} = \langle\psi_v|r|\psi_c\rangle$ is the dipole matrix element that characterizes the transition from the valence state v to the conduction state c. The transition energy is calculated using first-order perturbation theory as $E_{v,c} = \varepsilon_c - \varepsilon_v - J_{v,c}$, where $J_{v,c}$ is the electron−hole Coulomb interaction energy.[39]

Figure 6a shows the MEG rate for all four CdSe QDs as a function of the photon energy, $\hbar\omega$, calculated using eq 3. As expected from the results for the individual charge carriers (see, *e.g.*, Figure 2), the MEG rate increases with photon energy. The MEG rate also

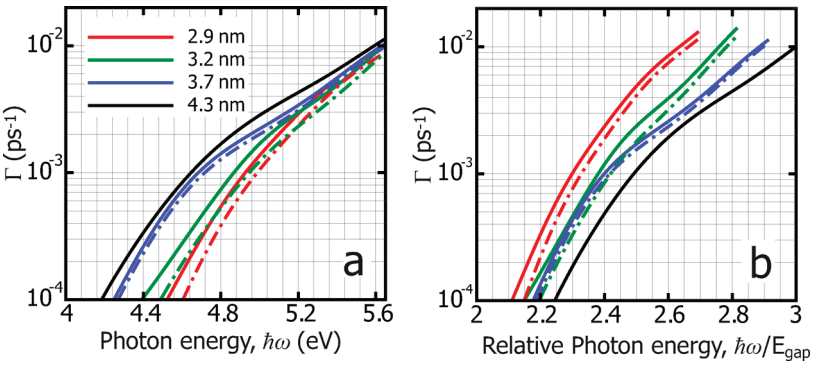

Figure 6. MEG rate (eq 3) as a function of (a) absolute photon energy and (b) relative photon energy scaled by the optical band gaps for four CdSe QDs. Dashed lines are calculated by including only the contribution from excited electrons, *i.e.*, Γ_e in eq 3. For the largest dot (4.3 nm), the MEG rate includes only the electron contribution, as the hole contribution is negligible (see text).

increases with QD size for a given photon energy (Figure 6a). The trend is just the opposite, though, if the relative photon energy $\hbar\omega/E_{gap}$ is kept fixed (Figure 6b). This is because quantum confinement causes the optical gap to increase with decreasing QD size so that the photon energy has to increase to keep the ratio $\hbar\omega/E_{gap}$ constant. The calculated MEG rate is relatively low (*e.g.*, $\Gamma < 10^{-2}$ ps^{-1} at $\hbar\omega = 2.7E_{gap}$ for the 3.2 nm QD). This result suggests that, at low photon energies, MEG can be easily overcome by competing carrier relaxation processes. This is in agreement with the experimental results of Nair *et al.*[14]

Figure 6 also makes clear that the main contribution to the total MEG rate originates from electrons decaying into negative trions. This is due to the asymmetrical distribution of dipole matrix elements in the optical transitions of CdSe QDs. As shown in Figure 7, in a photogenerated electron−hole pair, the electron has higher excess energy than the hole, so photoexcited electrons tend to have a much higher probability of decaying by MEG. This is so despite the fact that the MEG rate for an individual hole is larger than that of an electron with the same excess energy (Figure 2). If an excited electron could be efficiently converted to an excited hole through an Auger process, though, the total MEG rate could be significantly enhanced.

The dependence of the exciton MEG rate on volume can be quantified by fitting the results of Figure 6 to power law functions of the QD volume. These fits are given in Figure 8. We find that, for a given absolute photon energy, the MEG rate scales as $\Gamma = \Gamma_0 + \alpha V^{\beta}$, with β ranging from −0.70 to −0.91 in the energy range under consideration. In contrast, the MEG rate as a function of the relative photon energy scales as $\Gamma = \alpha V^{\beta}$, with β lying between −1.36 and −1.21 (Table 3). Nair *et al.*[14] argued that the MEG rate should not exhibit a significant volume dependence because of the offsetting volume dependencies of Coulomb coupling and density of states. Specifically, it was suggested that the average Coulomb coupling scales as V^{-4}, while the biexciton DOS scales as V^4. Our calculations show, however, that the volume dependence of the Coulomb

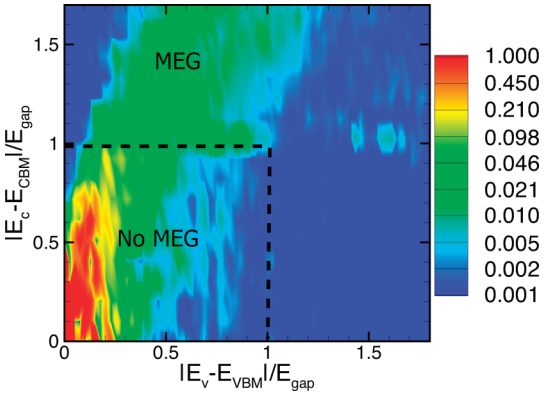

Figure 7. Distribution of the dipole matrix element amplitude (arbitrary units), $|M_{v,c}|^2$, in the optical transitions as a function of the electron and hole excess energies rescaled by the optical band gap E_{gap} for a 3.7 nm CdSe QD. The black dashed line delineates the region where MEG is not possible because of insufficient excess energy.

coupling between initial state and the final trion state is roughly V^{-3} for initial excited electrons but closer to V^{-4} for excited holes. The trion DOS scaling depends on volume as V^{α}, with α ranging from 3.1 to 4.1 for a negative trion and from 3.8 to 5.5 for a positive trion. These results show that the volume scaling contributions to MEG rate from the effective Coulomb coupling and trion DOS do not cancel each other and that there is an energy dependence that must be considered as well. The net scaling of the MEG rate is quantified in Figure 8 and Table 3.

The MEG rate has been plotted against both absolute and relative photon energy (Figure 6a,b). However, the relative data may be more relevant in assessing MEG *efficiency* since, for a given QY, the conversion efficiency increases with excitonic gap.[21,32] Beard *et al.*[47] have proposed a measure of MEG efficiency that is proportional to the slope of the QY *versus* the relative photon energy $\hbar\omega/E_{gap}$ (above the MEG threshold, $\hbar\omega_{th}$). Thus, the dependence of the MEG rate on QD volume calculated with respect to this relative photon energy (Figure 8b) is more appropriate to describe the trend of the MEG efficiency with QD size.

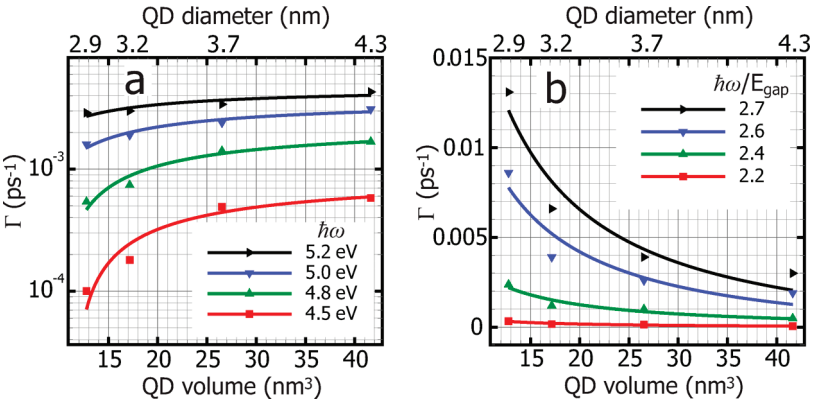

Figure 8. Volume dependence of the MEG rate of CdSe QDs, calculated (a) at fixed absolute photon energy and (b) at fixed relative photon energy scaled by the optical band gap. Solid lines are power law fits to the MEG rate for selected energies, and the resulting coefficients are collected in Table 3.

TABLE 3. Fitted Parameters for the Volume Dependence of MEG Rate: (Left) $\Gamma = \Gamma_0 + \alpha V^\beta$ at Given Absolute Photon Energy, $\hbar\omega$; (Right) $\Gamma = \alpha V^\beta$ at Given Photon Energy Scaled by the Optical Band Gap of the QD, $\hbar\omega/E_{gap}$, As Shown in Figure 6

$\hbar\omega$ (eV)	β	$\hbar\omega/E_{gap}$	β
4.5	−0.70	2.2	−1.36
4.8	−0.78	2.4	−1.21
5.0	−0.82	2.6	−1.20
5.2	−0.91	2.7	−1.21

In summary, we have applied an atomistic pseudopotential method to quantify the relation between size and MEG rate in CdSe QDs. Volume scaling laws for overall MEG, trion DOS, and Coulomb coupling integral have now been quantified under realistic conditions and with a minimal number of simplifying idealizations. Earlier estimates that the competing volume scaling effects of Coulomb coupling and density of states should cancel are shown to not be accurate. The MEG rate increases as the QD volume decreases if the comparison is made for the same relative photon energies, that is, after normalization using the volume-dependent optical gap. The opposite trend is found if the comparison is made using the same absolute photon energy for each QD. Both the effective Coulomb coupling and the trion DOS are energy dependent, with the latter being a stronger function of energy. Although the MEG rate of excited holes is much larger than that of excited electrons, the MEG rate of an electron−hole pair is dominated by the photoexcited electron. This is so because photoexcited electrons tend to have larger excess energy than photoexcited holes.

METHODS

Our computational approach utilizes an atomistic pseudopotential that is tailored to capture the experimental electronic structure of CdSe QDs .[34,35,39] The CdSe QDs are constructed by carving out a Se-centered sphere from bulk CdSe in the zinc blende structure. We use the experimental lattice constant $a_0 = 6.08$ Å.[40] The single-particle energies, ε_i, and wave functions, ψ_i, of the QD are obtained by solving the single-particle Schrödinger equation:

$$\left[-\frac{\hbar}{2m}\nabla^2 + V(\boldsymbol{r}) + \hat{V}_{SO}\right]\psi_i(\boldsymbol{r},\sigma) = \varepsilon_i\psi_i(\boldsymbol{r},\sigma) \quad (6)$$

where $\hat{V}_{SO}$ is the nonlocal spin−orbit operator[34] and the local potential, $V(\boldsymbol{r})$, is a linear superposition of screened atomic pseudopotentials centered at the atomic positions, $\{\boldsymbol{R}\}$:

$$V(\boldsymbol{r}) = \sum_{\alpha,R} v_\alpha(\boldsymbol{r} - \boldsymbol{R}) \quad (7)$$

The Cd and Se atomic pseudopotentials were fitted to experimental bulk CdSe properties, such as transition energies and effective masses, and to single-particle bulk wave functions calculated from first principles.[34,35] All surface Cd and Se atoms are passivated using ligand-like atomic pseudopotentials that are fitted to remove the surface states from the band gap of the QD.[34] The ligand potentials have the form

$$v_0 \exp\left(-\left(\frac{|\boldsymbol{r} - \boldsymbol{R}_0|}{0.79}\right)^2\right) \quad (8)$$

The origin, R_0, is centered along the directions of the dangling bonds at a distance d_0 from the surface Cd/Se atoms. The quantities d_0 and v_0 are fitting parameters.[34] The single-particle wave functions, ψ_i, are expanded in a plane wave basis set. The calculated optical band gap of the four zinc blende CdSe QDs in this work decreases from 2.14 eV (for the $D = 2.9$ nm QD) down to 1.86 eV ($D = 4.3$ nm), as shown in Table 4. The discrepancy between the calculated optical band gaps in this work and the experimentally reported values[36,37] is attributable to the underestimated bulk band gap from our pseudopotential approach, 1.61 eV, as compared to the experimental bulk band gap, 1.66 eV at room temperature, for zinc blende CdSe.[38]

The MEG rates for electrons and holes are calculated by applying Fermi's golden rule to the formation of trion states:

$$\Gamma_e = \frac{2\pi}{\hbar}\sum_f |\langle e|W|f\rangle|^2 \delta(E_f^- - E_e) \quad (9)$$

$$\Gamma_h = \frac{2\pi}{\hbar}\sum_f |\langle h|W|f\rangle|^2 \delta(E_f^+ - E_h) \quad (10)$$

Here $|e\rangle$ and $|h\rangle$ are the initial excited states for an electron in the conduction band and a hole in the valence band, respectively.

TABLE 4. Screened Coulomb Energies, $J_{i,j}$, and Optical Gaps, E_{gap}, (in eV) of the Four CdSe QDs Considered in This Study

size (nm)	$J_{VBM,VBM}$	$J_{VBM,CBM}$	$J_{CBM,CBM}$	E_{gap}
2.9	0.33	0.27	0.24	2.14
3.2	0.28	0.23	0.21	2.05
3.7	0.23	0.19	0.17	1.95
4.3	0.20	0.16	0.14	1.86

The operator, W, is the screened Coulomb matrix element between the initial and final states.[41,43,44] The final trion states of eqs 9 and 10 are $|f^-\rangle = |e_1,e_2,h_1\rangle$ and $|f^+\rangle = |e_1,h_1,h_2\rangle$, respectively. Their energies are calculated as

$$E_f^- = (\varepsilon_{e1} + \varepsilon_{e2} - \varepsilon_{h1}) + (J_{e1,e2} - J_{e1,h1} - J_{e2,h1}) \quad (11)$$

and

$$E_f^+ = (\varepsilon_{e1} - \varepsilon_{h1} - \varepsilon_{h2}) + (J_{h1,h2} - J_{e1,h1} - J_{e1,h2}) \quad (12)$$

The screened Coulomb interaction, $J_{i,j}$, between single-particle state i and j is given by

$$J_{i,j} = \sum_{\sigma,\sigma'} \int\int d\mathbf{r}d\mathbf{r}' |\psi_i(\mathbf{r}',\sigma')|^2 \frac{e^2}{\varepsilon(\mathbf{r},\mathbf{r}')|\mathbf{r}-\mathbf{r}'|} |\psi_j(\mathbf{r},\sigma)|^2 \quad (13)$$

where $\varepsilon(\mathbf{r},\mathbf{r}')$ is the dielectric screening function of the QD.[39] Table 4 shows the screened Coulomb energies between VBM and CBM states in all four CdSe QDs considered in this study. We adopt a Lorentzian line shape

$$\delta(E_f - E_i) \rightarrow \frac{1}{\pi} \frac{(\gamma/2)}{(E_i - E_f)^2 + (\gamma/2)^2} \quad (14)$$

in evaluating eq 9 and eq 10, to account for phonon broadening effects. A value of $\gamma = 10$ meV is used for the summation over the final states;[44] changes in γ from 5 to 20 meV were found to not meaningfully affect MEG rates.

Our pseudopotential method is similar to that used by Rabani *et al.*[25,26] to calculate the MEG rates of small (up to ~500 atoms) CdSe nanocrystals. We build on their work by (i) examining larger (up to ~1500 atoms) CdSe QDs; (ii) including spin−orbit coupling, which is important in CdSe QDs[34] for describing states at the top of valence band, which participate significantly in the MEG process; and (iii) including excitonic interactions in the calculation of the MEG rates (eq 11 and eq 12).

The importance of including excitonic interactions in calculating the MEG rates is shown in Figure 9. Electron−hole Coulomb interactions (eq 13) lower the energy of the final (trion) states (see eq 11 and eq 12), thereby increasing the density of final states that are in resonance with the initial state. As shown in Figure 9a, the net result is an overall increase in the MEG rate as compared with the case where these Coulomb interactions are neglected. The difference can be significant, nearly an order of magnitude at low excess energies when the excitonic effects are taken into account. Interestingly, if the excess energy is rescaled by the appropriate band gap (the optical band gap when excitonic interactions are included, and $\varepsilon_{CBM}-\varepsilon_{VBM}$ when they are not), then the MEG rates calculated with and without excitonic effects are nearly the same (Figure 9b). This is due to the fact that, while the final trion energies (eq 11 and eq 12) are reduced by the excitonic interactions, the optical gap is reduced by a similar amount.

Acknowledgment. We are grateful to A. Nozik and M. Beard for useful discussions concerning MEG efficiency. This work was supported by the Renewable Energy Materials Research Science and Engineering Center (NSF Grant No. DMR-0820518) at the Colorado School of Mines and the National Renewable Energy Laboratory (NREL). The calculations were carried out using the high performance computing resources provided by the Golden Energy Computing Organization at the Colorado School of Mines (NSF Grant No. CNS-0722415).

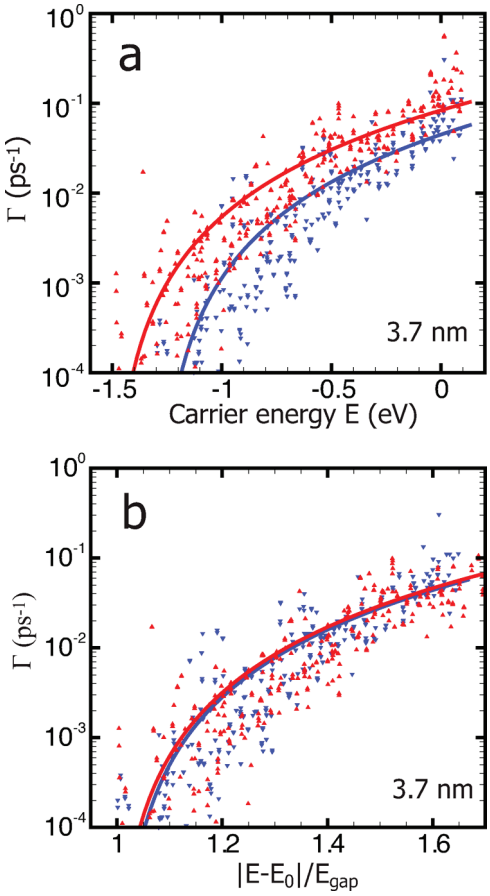

Figure 9. Comparison of MEG rates for electrons in 3.7 nm CdSe QD with (red) and without (blue) excitonic interactions (eq 9). Data points and fitted curves are shown in the same way as in Figure 2.

REFERENCES AND NOTES

1. Nozik, A. J. Spectroscopy and Hot Electron Relaxation Dynamics in Semiconductor Quantum Wells and Quantum Dots. *Annu. Rev. Phys. Chem.* **2001,** *52*, 193–231.
2. Nozik, A. J. Quantum Dot Solar Cells. *Physica E* **2002,** *14*, 115–120.
3. Schaller, R. D.; Klimov, V. I. High Efficiency Carrier Multiplication in PbSe Nanocrystals: Implications for Solar Energy Conversion. *Phys. Rev. Lett.* **2004,** *92*, 186601-1–186601-4.
4. Ellingson, R. J.; Beard, M. C.; Johnson, J. C.; Yu, P. R.; Micic, O. I.; Nozik, A. J.; Shabaev, A.; Efros, A. L. Highly Efficient Multiple Exciton Generation in Colloidal PbSe and PbS Quantum Dots. *Nano Lett.* **2005,** *5*, 865–871.
5. Schaller, R. D.; Petruska, M. A.; Klimov, V. I. Effect of Electronic Structure on Carrier Multiplication Efficiency: Comparative Study of PbSe and CdSe Nanocrystals. *Appl. Phys. Lett.* **2005,** *87*, 253102-1–253102-3.
6. Schaller, R. D.; Agranovich, V. M.; Klimov, V. I. High-Efficiency Carrier Multiplication through Direct Photogeneration of Multi-excitons *via* Virtual Single-Exciton States. *Nat. Phys.* **2005,** *1*, 189–194.
7. Schaller, R. D.; Klimov, V. I. Non-Poissonian Exciton Populations in Semiconductor Nanocrystals *via* Carrier Multiplication. *Phys. Rev. Lett.* **2006,** *96*, 097402-1–097402-4.
8. Murphy, J. E.; Beard, M. C.; Norman, A. G.; Ahrenkiel, S. P.; Johnson, J. C.; Yu, P. R.; Micic, O. I.; Ellingson, R. J.; Nozik, A. J. PbTe Colloidal Nanocrystals: Synthesis, Characterization, and Multiple Exciton Generation. *J. Am. Chem. Soc.* **2006,** *128*, 3241–3247.
9. Schaller, R. D.; Sykora, M.; Jeong, S.; Klimov, V. I. High-Efficiency Carrier Multiplication and Ultrafast Charge

Separation in Semiconductor Nanocrystals Studied *via* Time-Resolved Photoluminescence. *J. Phys. Chem. C* **2006,** *110*, 25332–25338.
10. Beard, M. C.; Knutsen, K. P.; Yu, P.; Luther, J. M.; Song, Q.; Metzger, W. K.; Ellingson, R. J.; Nozik, A. J. Multiple Exciton Generation in Colloidal Silicon Nanocrystals. *Nano Lett.* **2007,** *7*, 2506–2512.
11. Schaller, R. D.; Pietryga, J. M.; Klimov, V. I. Carrier Multiplication in InAs Nanocrystal Quantum Dots with an Onset Defined by the Energy Conservation Limit. *Nano Lett.* **2007,** *7*, 3469–3476.
12. Luther, J. M.; Beard, M. C.; Song, Q.; Law, M.; Ellingson, R. J.; Nozik, A. J. Multiple Exciton Generation in Films of Electronically Coupled PbSe Quantum Dots. *Nano Lett.* **2007,** *7*, 1779–1784.
13. Nair, G.; Bawendi, M. G. Carrier Multiplication Yields of CdSe and CdTe Nanocrystals by Transient Photoluminescence Spectroscopy. *Phys. Rev. B* **2007,** *76*, 081304-1–081304-4.
14. Nair, G.; Geyer, S. M.; Chang, L.-Y.; Bawendi, M. G. Carrier Multiplication Yields in PbS and PbSe Nanocrystals Measured by Transient Photoluminescence. *Phys. Rev. B* **2008,** *78*, 125325-1–125325-10.
15. Trinh, M. T.; Houtepen, A. J.; Schins, J. M.; Hanrath, T.; Piris, J.; Knulst, W.; Goossens, A. P. L. M.; Siebbeles, L. D. A. In Spite of Recent Doubts Carrier Multiplication Does Occur in PbSe Nanocrystals. *Nano Lett.* **2008,** *8*, 1713–1718.
16. Mcguire, J. A.; Joo, J.; Pietryga, J. M.; Schaller, R. D.; Klimov, V. I. New Aspects of Carrier Multiplication in Semiconductor Nanocrystals. *Acc. Chem. Res.* **2008,** *41*, 1810–1819.
17. Ben-Lulu, M.; Mocatta, D.; Bonn, M.; Banin, U.; Ruhman, S. On the Absence of Detectable Carrier Multiplication in a Transient Absorption Study of InAs/CdSe/ZnSe Core/Shell1/Shell2 Quantum Dots. *Nano Lett.* **2008,** *8*, 1207–1211.
18. Beard, M. C.; Midgett, A. G.; Law, M.; Semonin, O. E.; Ellingson, R. J.; Nozik, A. J. Variations in the Quantum Efficiency of Multiple Exciton Generation for a Series of Chemically Treated PbSe Nanocrystal Films. *Nano Lett.* **2009,** *9*, 836–845.
19. Pijpers, J. J. H.; Ulbricht, R.; Tielrooij, K. J.; Osherov, A.; Golan, Y.; Delerue, C.; Allan, G.; Bonn, M. Assessment of Carrier-Multiplication Efficiency in Bulk PbSe and PbS. *Nat. Phys.* **2009,** *5*, 811–814.
20. Ji, M.; Park, S.; Connor, S. T.; Mokari, T.; Cui, Y.; Gaffney, K. J. Efficient Multiple Exciton Generation Observed in Colloidal PbSe Quantum Dots with Temporally and Spectrally Resolved Intraband Excitation. *Nano Lett.* **2009,** *9*, 1217–1222.
21. McGuire, J.; Sykora, M.; Joo, J.; Pietryga, J.; Klimov, V. I. Apparent *versus* True Carrier Multiplication Yields in Semiconductor Nanocrystals. *Nano Lett.* **2010,** *10*, 2049–2057.
22. Wang, S.; Khafizov, M.; Tu, X.; Zheng, M.; Krauss, T. D. Multiple Exciton Generation in Single-Walled Carbon Nanotubes. *Nano Lett.* **2010,** *10*, 2381–2386.
23. Schaller, R. D.; Sykora, M.; Pietryga, J. M.; Klimov, V. I. Seven Excitons at a Cost of One: Redefining the Limits for Conversion Efficiency of Photons into Charge Carriers. *Nano Lett.* **2006,** *6*, 424–429.
24. Franceschetti, A.; Zhang, Y. Multiexciton Absorption and Multiple Exciton Generation in CdSe Quantum Dots. *Phys. Rev. Lett.* **2008,** *100*, 136805-1–136805-4.
25. Rabani, E.; Baer, R. Distribution of Multiexciton Generation Rates in CdSe and InAs Nanocrystals. *Nano Lett.* **2008,** *8*, 4488–4492.
26. Rabani, E.; Baer, R. Theory of Multiexciton Generation in Semiconductor Nanocrystals. *Chem. Phys. Lett.* **2010,** *496*, 227–235.
27. Isborn, C. M.; Kilina, S. V.; Li, X.; Prezhdo, O. V. Generation of Multiple Excitons in PbSe and CdSe Quantum Dots by Direct Photoexcitation: First-Principles Calculations on Small PbSe and CdSe Clusters. *J. Phys. Chem. C* **2008,** *112*, 18291–18294.
28. Fischer, S. A.; Madrid, A. B.; Isborn, C. M.; Prezhdo, O. V. Multiple Exciton Generation in Small Si Clusters: A High-Level, *Ab Initio* Study. *J. Phys. Chem. Lett.* **2010,** *1*, 232–237.
29. Isborn, C. M.; Prezhdo, O. V. Charging Quenches Multiple Exciton Generation in Semiconductor Nanocrystals: First-Principles Calculations on Small PbSe Clusters. *J. Phys. Chem. C* **2009,** *113*, 12617–12621.
30. Kilina, S.; Ivanov, S.; Tretiak, S. Effect of Surface Ligands on Optical and Electronic Spectra of Semiconductor Nanoclusters. *J. Am. Chem. Soc.* **2009,** *131*, 7717–7726.
31. Madrid, A. B.; Hyeon-Deuk., K; Habenicht, B. F.; Prezhdo, O. V. Phonon-Induced Dephasing of Excitons in Semiconductor Quantum Dots: Multiple Exciton Generation, Fission, and Luminescence. *ACS Nano* **2009,** *3*, 2487–2494.
32. Delerue, C.; Allan, G.; Pijpers, J. J. H.; Bonn, M. Carrier Multiplication in Bulk and Nanocrystalline Semiconductors: Mechanism, Efficiency, and Interest for Solar Cells. *Phys. Rev. B* **2010,** *81*, 125306-1–125306-6.
33. Smith, A.; Dutton, D. Behavior of Lead Sulfide Photocells in the Ultraviolet. *J. Opt. Soc. Am.* **1958,** *48*, 1007–1009.
34. Wang, L. W.; Zunger, A. Pseudopotential Calculations of Nanoscale CdSe Quantum Dots. *Phys. Rev. B* **1996,** *53*, 9579–9582.
35. Wang, L. W.; Zunger, A. High-Energy Excitonic Transitions in CdSe Quantum Dots. *J. Phys. Chem. B* **1998,** *102*, 6449–6454.
36. Yu, W.; Qu, L.; Guo, W.; Peng, X. Experimental Determination of the Extinction Coefficient of CdTe, CdSe, and CdS Nanocrystals. *Chem. Mater.* **2003,** *15*, 2854–2860.
37. Wang, Q.; Seo, D.-K. Synthesis of Deep-Red-Emitting CdSe Quantum Dots and General Non-Inverse-Square Behavior of Quantum Confinement in CdSe Quantum Dots. *Chem. Mater.* **2006,** *18*, 5764–5767.
38. Shan, W.; Song, J. J.; Luo, H.; Furdyna, J. K. Determination of the Fundamental and Split-Off Band Gaps in Zinc-Blende CdSe by Photomodulation Spectroscopy. *Phys. Rev. B* **1994,** *50*, 8012–8015.
39. Franceschetti, A.; Fu, H.; Wang, L. W.; Zunger, A. Many-Body Pseudopotential Theory of Excitons in InP and CdSe Quantum Dots. *Phys. Rev. B* **1999,** *60*, 1819–1829.
40. Kaxiras, E. *Atomic and Electronic Structure of Solids*; Cambridge University Press: Cambridge, U.K., 2003.
41. Kane, E. O. Electron Scattering by Pair Production in Silicon. *Phys. Rev.* **1967,** *159*, 624–631.
42. Allan, G.; Delerue, C. Role of Impact Ionization in Multiple Exciton Generation in PbSe Nanocrystals. *Phys. Rev. B* **2006,** *73*, 205423-1–205423-5.
43. Landsberg, P. *Recombination in Semiconductors*; Cambridge University Press: Cambridge, U.K., 1991.
44. Wang, L. W.; Califano, M.; Zunger, A.; Franceschetti, A. Pseudopotential Theory of Auger Processes in CdSe Quantum Dots. *Phys. Rev. Lett.* **2003,** *91*, 056404-1–056404-4.
45. Franceschetti, A.; An, J. M.; Zunger, A. Impact Ionization Can Explain Carrier Multiplication in PbSe Quantum Dots. *Nano Lett.* **2006,** *6*, 2191–2195.
46. Allan, G.; Delerue, C. Influence of Electronic Structure and Multiexciton Spectral Density on Multiple-Exciton Generation in Semiconductor Nanocrystals: Tight-Binding Calculations. *Phys. Rev. B* **2008,** *77*, 125340-1–125340-10.
47. Beard, M. C.; Midgett, A. G.; Hanna, M. C.; Luther, J. M.; Hughes, B. K.; Nozik, A. J. Comparing Multiple Exciton Generation in Quantum Dots To Impact Ionization in Bulk Semiconductors: Implications for Enhancement of Solar Energy Conversion. *Nano Lett.* **2010,** *10*, 3019–3027.